International Journal of Applied Earth Observations and Geoinformation 103 (2021) 102525

Contents lists available at ScienceDirect

International Journal of Applied Earth Observations and Geoinformation

journal homepage: www.elsevier.com/locate/jag

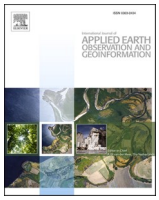

Spatio-temporal changes in urban green space in 107 Chinese cities (1990–2019): The role of economic drivers and policy

Wan-Ben Wu [a], Jun Ma [a], Michael E. Meadows [c], Ellen Banzhaf [b], Tian-Yuan Huang [d], Yi-Fei Liu [a], Bin Zhao [a,*]

[a] Ministry of Education Key Laboratory for Biodiversity Science and Ecological Engineering, Coastal Ecosystems Research Station of the Yangtze River Estuary, and Shanghai Institute of EcoChongming (SIEC), Fudan University, Shanghai 200433, China
[b] UFZ - Helmholtz Centre for Environmental Research, Department of Environmental Sociology, Leipzig, Germany
[c] Department of Environmental & Geographical Science, University of Cape Town, Cape Town 7701, South Africa
[d] National Science Library, Chinese Academy of Sciences, China

ARTICLE INFO

Keywords:
Normalized Urban Development Index
Regional Greenness Dynamic Index
Urbanisation
Google Earth Engine
Night-time light

ABSTRACT

Urban green space (UGS) has gained increasing attention due to its environmental and social functions. However, the compound effects of climate change, population growth and economic development on UGS are largely unknown. We selected 107 medium-sized and large cities in China to investigate dynamics in the spatial pattern of UGS in relation to government policy and other drivers based on remote sensing data for the period 1990 to 2019. To explore the effect of different levels of urbanization on changes in green space, we develop a new Normalized Urban Development Index (NUDI) to classify urban-suburban-rural gradients, viz. Long-term Built-up, New Built-up and Non-Built-up. Then, we analysed changes over time in the annual peak value of fraction of vegetation cover (FVC) for 380,000 cloud-free Landsat images, and regional UGS dynamics were evaluated using the proposed Regional Greenness Dynamic Index (RGDI). Finally, to reveal the major driver(s) of changes in UGS and estimate the extent to which patterns of urban greening are due to differences in economic development, we compared the observed UGS spatio-temporal dynamics with data on several climatic, social-economic and land use related factors for the same period. The NUDI are shown to be highly effective in mapping urban development gradients, with overall accuracy in the identified classes of 89%. Annual maximum FVC analysis indicates that there was significant greening between 1990 and 2019 in both the long-term built up (10,667.52 km^2) and the non-built up areas (529,310.47 km^2), while there was a major increase in browning (25,110.43 km^2) in the newly built-up areas. The RGDI results indicate that 65% (71/107) of long-term built-up areas in cities trended greener over 2010 to 2019 under consideration. At the whole city scale, RGDI is negatively correlated with gross domestic product (GDP), although when considering the long-term built-up areas only, economic growth exhibits a significant positive correlation during 2010 to 2019 ($R = 0.62$, $p < 0.01$). This study offers important insights as to the patterns of change in urban greening extent over time and its underyling drivers across urban-suburban-rural gradients against the background of urban expansion, afforestation, climate change and economic development.

1. Introduction

Urban Green Space (UGS) has multiple environmental benefits that include ameliorating air quality (Jeanjean et al., 2016), urban heat island mitigation (Du et al., 2017), and flood prevention (Bai et al., 2018). Previous research has demonstrated that improved access to UGS can also support mental health among the urban population (Chang et al., 2017; Hedblom et al., 2019). Ongoing urbanization demands appropriate provision of ecosystem services (Silvennoinen et al., 2017) and increasing the area and range of types of UGS have emerged as important means to improving environmental quality in cities, thereby contributing to urban sustainable development.

Following China's reform and opening-up policy, the urbanization rate tripled between 1978 and 2016 from 17.9 % to 57.4%. Extremely

* Corresponding author at: Ministry of Education Key Laboratory for Biodiversity Science and Ecological Engineering, School of Life Sciences, Fudan University, Shanghai 200433, China.
E-mail address: zhaobin@fudan.edu.cn (B. Zhao).

https://doi.org/10.1016/j.jag.2021.102525
Received 7 June 2021; Received in revised form 25 August 2021; Accepted 26 August 2021
Available online 3 September 2021

rapid growth has been accompanied by numerous environmental challenges, especially for remaining natural habitats, biodiversity, local and regional climate, as well as for UGS itself (Kalnay and Cai, 2003; Yang et al., 2017). In response to the various pressures associated with urban expansion and climate change on China's ecological situation, the Chinese government has promulgated a series of environmental policies. Urban re-greening and restoration of UGS and biodiversity are major thrusts of this policy. However, there are differences in urban responses to policies, while exhibiting unevenness and gradients in green space development. Studying the relationship between UGS and policy in China can be a good way to explore the mechanisms of policy influence on urban land use change and its ecological effects.

Remote sensing technologies provide a powerful spatial tool to evaluate change over time, particularly in relation to vegetation dynamics. Indices derived from satellite data, such as the normalized vegetation index (NDVI) and Leaf area index (LAI) are widely used to detect changes in greenness at a range of spatial scales. At the global scale, based on a long-term NDVI series, Myneni *et al.*(Myneni et al., 1997) revealed significantly increased vegetation greenness across the Northern Hemisphere from 1981 to 1991. Using LAI data from 2000 to 2016, Chen et al. (Chen et al., 2019) reported a markedly positive trend in vegetation greenness in China and India. On the other hand, between 2000 and 2016, Enhanced Vegetation Index (EVI) and GPP results for suburban and rural areas of Shanghai showed a downward trend of 38.0% and 28.0%, respectively, while the same measures exhibited an upward trend (2.8% and 4.6%, respectively) in the central parts of the city (Zhong et al., 2019).

Urban green space development is driven by both natural environmental factors and human activities (Barbosa et al., 2007; Xu et al., 2019). Natural factors affect the distribution of UGS by influencing the distribution, survival and reproduction of vegetation (Weng et al., 2021). For example, topography, moisture, air quality, precipitation, temperature and radiation all affect the distribution of UGS (Rupprecht et al., 2015; McPhearson et al., 2013; Piao et al., 2020). The influence of human activities on UGS includes population density, policy and urbanization (Kabisch et al., 2016; Richards et al., 2017). Previous studies have demonstrated that the process of urbanization has a significant effect on UGS dynamics (Zhou and Wang., 2011; Zhou et al., 2016), but the majority of these are at the scale of a single city or for a single year and use a range of different measures. Most of these studies also analyse urban greening trends based on established administrative boundaries which do not adequately represent the development stage of each city, and are therefore not suited to studying differences in the distribution of green space along the urban centre/suburban/rural gradient.

In the context of rapid urbanization and economic development in China, the question then arises as to the nature and scale of UGS in cities in relation to the greening policies. In this study we aim to explore trends in UGS in Chinese cities at a range of development stages and urban–rural gradients with a view to determining the main driving forces underlying the observed spatio-temporal patterns. In approaching this complex issue in a spatially explicit way, we utilize remote sensing techniques and published statistics relating to economic activities and formulate the following objectives for 107 medium and large Chinese cities; a) to quantify, using a time series of night time light images, spatio-termporal trends in urban development; b) to assess spatial dynamics of UGS in each of the urban development zones; c) to develop a comprehensive indicator to quantify the degree of change in UGS at the regional scale.

2. Materials

2.1. Study area

Those Chinese cities with a population of greater than 5 million inhabitants (based on 2018 Chinese government city statistical data) are regarded as highly developed, yielding 107 urban agglomerations which form the basis this study. Most of these cities are located in the eastern and north-eastern regions of the country (Fig. 1), the largest of which is Shanghai (with c. 25 million. Inhabitants). The urban population of these 107 cities represents 67% of the total population of China.

2.2. Data

2.2.1. Night-time light images

The stable Defense Meteorological Satellite Program-Operational Linescan System night-time light data (DMSP-OLS-NTL) has outstanding potential to accurately map the urban extent. NTL is widely used to provide information about urbanization processes and to evaluate the location and dimension of urban agglomerations, including impervious surface area, population density, GDP, and the form of the urban boundary (Elvidge et al., 2007; Zhou et al., 2008; Liu et al., 2015). In this study, we used long-term annual NTL data from 1992 to 2013 to construct a novel index, named here as the Normalized Urban Development Index (NUDI. Due to variations in atmospheric conditions over time, DMSP-OLS-NTL data were normalized using Eq. (1). OLS_{nor} can reduce the effect of NTL saturation and also increase the variability of NTL signal in urban areas (Zhang et al., 2013). All datasets were resampled to the same spatial resolution (300 m) using the nearest-neighbour resampling algorithm.

$$OLS_{nor} = \left(\frac{OLS - OLS_{min}}{OLS_{max} - OLS_{min}}\right)(1 - NDVI_{max}) \quad (1)$$

Where OLS_{nor} is the normalized DMSP-OLS-NTL pixel value, and OLS_{max} and OLS_{min} represent the regional maximum and minimum values in the DMSP-OLS-NTL image of each city, respectively.

2.2.2. Landsat imagery

Surface reflectance products of 380,000 images covering the period 1990 to 2019 at 16 days temporal were extracted from the Landsat series in GEE. Both the Landsat datasets and the pre-processing algorithm used in this study are available on the GEE platform. The availability of suitable images of Landsat-5/7/8 data are shown in Fig. 2 (a), and the distribution of data used in each year is depicted in Fig. 2 (b). We calculated two greenness-related spectral indices, including the Normalized Difference Vegetation Index (NDVI) (Goward et al., 1991) and the Fraction of Vegetation Cover (FVC) (Gutman and Ignatov, 1998). In order to reduce the effect of differential sensor calibration in Landsat 5/7/8, the annual peak NDVI ($NDVI_{max}$), and its derived FVC, were utilized to assess UGS dynamics, whichwere calculated using Eq. (2).

$$\mathrm{NDVI} = \frac{\rho_{NIR} - \rho_{red}}{\rho_{NIR} + \rho_{red}} \quad (2a)$$

$$NDVI_{max} = Maximum[NDVI_1, NDVI_2, \cdots, NDVI_n] \quad (2b)$$

$$\mathrm{FVC} = \frac{NDVI - NDVI_s}{NDVI_v + NDVI_s} \quad (2c)$$

Where ρ_{red} and ρ_{NIR}represent the surface reflectance, corresponding to the red band and near-infrared band, respectively. $NDVI_{max}$ represents the annual maximum NDVI values for the respective time series,$NDVI_1, NDVI_2, \cdots, NDVI_n$ are the calculated indices for all Landsat time series.$NDVI_v$and $NDVI_s$ are the NDVI fractions of the complete vegetation canopy and bare soil, respectively.

2.2.3. Meteorological data

The China Meteorological Forcing Dataset (CMFD) is a gridded near-surface meteorological dataset, developed specifically for the study of land-surface processes in China (He et al., 2020). In this study, annual mean near-surface air temperature (AMT), annual mean downward shortwave radiation (AMSR), annual mean downward longwave radiation (AMLR), and annual total precipitation (ATP) were used as the

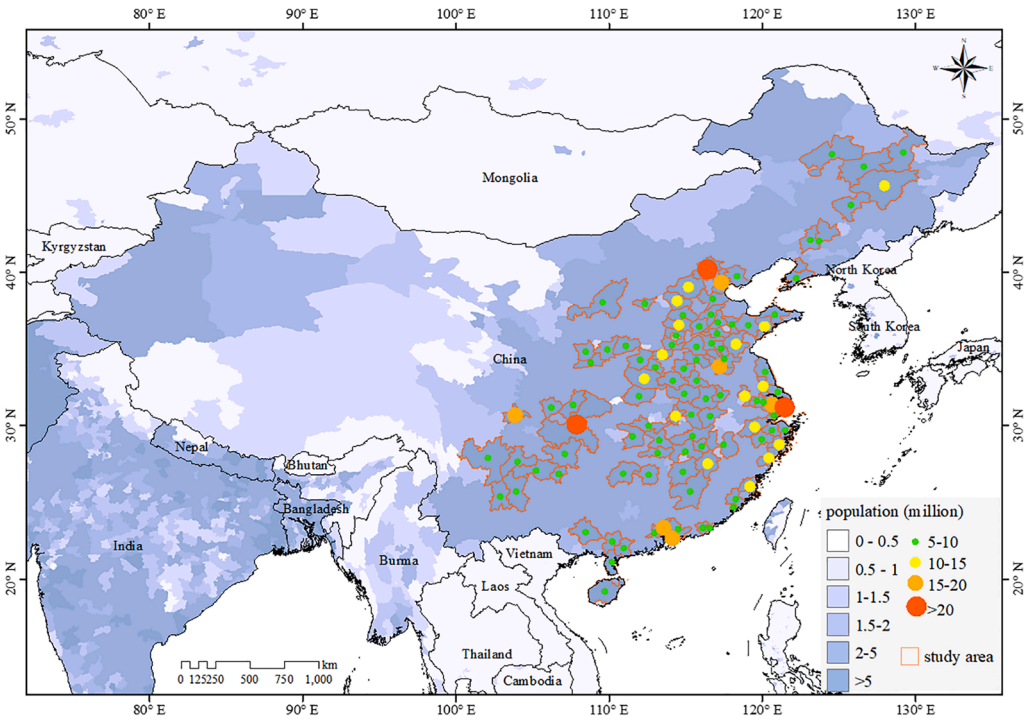

Fig. 1. Overview of the study area showing the location and population of the 107 cities included in the study.

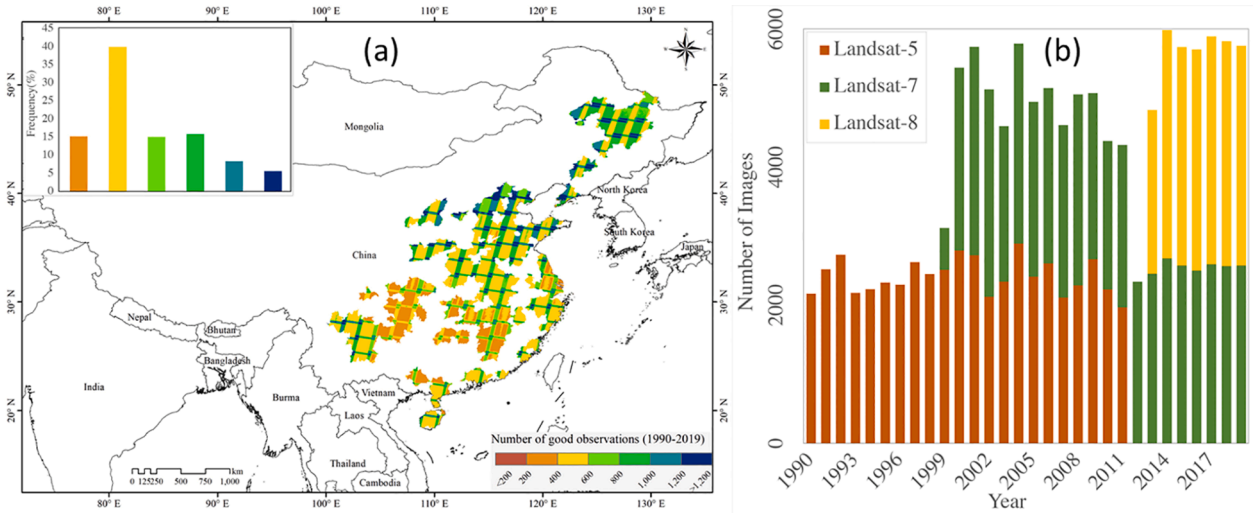

Fig. 2. (a) shows the number of suitable images from 1990 to 2019, and (b) shows the distribution of Landsat 5/7/8 data volumes available for each year.

climatic factors to compare with UGS dynamics. The dataset was provided by the National Tibetan Plateau Data Centre (http://data.tpdc.ac.cn).

2.2.4. Socio-economic data

Population figures and gross domestic product values (denoted as POP, GDP, respectively) are representative of urbanization and economic growth for each city. The POP and GDP datasets were obtained from the online local annual statistical yearbooks (http://tongji.cnki.net/).

2.2.5. The global artificial impervious areas (GAIA)

We obtained the 2018 urban map using global artificial impervious areas (GAIA) dataset (Gong et al., 2020) and used this as the current urban distribution base map to help classify the urban area into different development zones. Furthermore, the annual urban area extent was obtained for each city based on GAIA to calculate the ratio of impervious surface coverage (ISC) as an important factor influencing UGS. GAIA products are available at http://data.ess.tsinghua.edu.cn/gaia.html.

3. Methods

3.1. Algorithms for urban development zone identification

In order to better understand the effect of urbanization on UGS dynamics, we classify the urban area into three different urban development zones viz. long-term built-up (LB), new built-up (NewB), and non-built-up (NB) using a cluster-based method. Firstly, we reclassified city area into built-up and non-built-up region with the help of the current urban distribution map (based on GAIA product in 2018). Secondly, we

developed a novel index, the Normalized Urban Development index (NUDI) to qualify the degree of urban development, calculated as per Eq. (3). The main principle of the NUDI is to further distinguish long-term built-up areas from new built-up areas by quantifying the stability of nigh-time light intensity, so a larger $OLS_{max} - OLS_{min}$ in NUDI indicates that the night-time light intensity in the area has increased significantly within a certain time frame, and the greater the likelihood that it is a new built-up area, otherwise it is long-term built-up area. Eq. (3)

$$NUDI = \frac{OLS_{max} - OLS_{min}}{OLS_{max} + OLS_{min}} \quad (3)$$

Where OLS_{max} is the maximum value of annual mean NTL time series over the period in question, OLS_{min} is the minimum value of annual mean NTL time series over the period.

Based on the NUDI results and the known urban distribution, the three different development zones for each city were identified using Eq. (4). In order to fill inner pixels in Long-term built-up and New built-up zones, a kernel density estimation combined with morphological approach (Li et al. 2020) was used was used to fill the gaps to derive the built-up areas of the different zones.

Eq. (4)

$$\begin{cases} NUDI < TandUrban_{current} = 1Long - termbuilt - Up \\ NUDI > TandUrban_{current} = 1Newbuilt - Up \\ Urban_{current} = 0Non - built - Up \end{cases} \quad (4)$$

Where $Urban_{current}$ represents the urban distribution in 2018 based on the GAIA product, used as currently built area mask to distinguish the built-up and non-built-up area. T represents the threshold for each city, which was automatically calculated using the Otsu algorithm for each city (Otsu et al., 1979).

To validate the accuracy of urban development zone classification, the total of 986 validation samples (including 332, 334, 320 samples for long-term built-up, new built-up and non-built-up, respectively) were collected with the help of high-resolution satellite image from Google Earth platform and global urban boundary (GUB) product. The confusion matrix method was used for validation.

3.2. Spatial-temporal dynamics in UGS, 1990–2019

The trend in FVC over a given period was calculated using the linear least squares regression of annual FVC values against time, and the significance of the trend was estimated by applying the Mann-Kendall statistical test. Moreover, a novel index, the Regional Greenness Dynamic Index (RGDI) was proposed to evaluate greenness dynamics, considering both the rate and area of greenness/brownness change for each pixel with values calculated as positive or negative (%m2) as per Eq. (5). RGDI values greater than 0 indicate that the region is characterized in general by greening, while negative values indicate overall browning.

$$RGDI = \sum_{i=1}^{n} Tr_i A_i N_{yr} \quad (5)$$

Where i represents the pixel with a significant trend, n is the total number of pixels in the region, such as long-term built-up, new built-up and non-built-up, Tr_i is the trend value of the pixel, A_i is the area of the pixel, and N_{yr} is the length of the study period.

3.3. Analysis of driving forces of UGS

Here, we selected seven variables as potential driving factors, including four factors related to climatic change (AMT, ATP, AMSR, AMLR), one factor related to land-use change (ISC), and two socio-economic factors (GDP and POP). Generalized linear models (GLM) was applied to assess the strength of the relationships between UGS and its driving factors. To assure statistical independence, highly correlated variables (Spearman's ρ greater than 0.8) were not applied in the same model. To explore the relative influence of each factor, a boosted regression tree (BRT) model was utilized. The four parameters of the BRT model, *viz*. The learning rate, tree complexity, number of trees and bag fraction, were set to 0.001, 6, 1000 and 0.75, respectively. BRT model was fitted using the dismo package (https://cran.r-project.org/web/packages/dismo/index.html) in R.

4. Results

4.1. Urban zonation

The temporal dynamics of urban expansion, detected using changes in long-term built-up and new built-up using the annual GAIA product, were assessed from 1990 to 2018. Fig. 3 provides examples of the urban zonation distribution for six major cities, viz. Shanghai, Beijing, Guangzhou, Wuhan, Xi'an, and Fuzhou city. Validation of the confusion matrix algorithm with the help of selected sample points reveal that the overall accuracy of urban zoning using NUDI and the threshold algorithm was 89%.

4.2. Zonal differences in UGS dynamics

Fig. 4 illustrates the greening and browning trends for six Chinese major, where long-term built-up urban areas are characterized by a general greening trend, while the new built-up spaces were subject to browning, and non-built-up areas trended markedly greener. However, the temporal dynamics of UGS varies greatly between zones and periods. More specifically, a significant browning trend in the long-term built-up urban areas of the six selected large cities is evident between 1990 and 2009 but this is followed by predominant greening from 2010 to 2019. In the new built-up category, it shows significant browning over 1990 to 2019, while non-built-up urban areas are associated with greening over the same time. Table 1 shows the statistics on the sum of significant green(SG) area and significant brown(SB) area in different zones for 107 cities.

In applying the rule RGDI greater than 0 = greening, RGDI < 0 = browning, we detected the degree of greening/browning for 107 cities over time (Fig. 5). In the long-term built-up zone, the area that was characterized by browning in each of the first two decades of the study period was greater than that which experienced greening. However, between 2010 and 2019 showed these areas in general became significantly greener overall. In the new built-up zone, the area subject to browning exceeds that which became greener. Finally, in non-developed zones, all time periods indicate significant greening. Fig. 6 shows the number of green and brown cities in different regions during the four time periods.

Between 1990 and 1999, the long-term built-up zones in all 107 were characterized by browning. In the following decade, the long-term built-up zone of 16 cities trended greener, and greening was prominent from 2010 to 2019 in the same zone in 71 of the cities. In the new built-up zone, only 12, 8 and 25 cities exhibited greening over the periods 1990 to 1999, 2000 to 2009 and 2010 to 2019 respectively. On the other hand, greening dominated the non-built up zones in 64, 76 and 85 of the cities for the same periods.

4.3. Factors driving UGS dynamics

We investigated the sensitivity of UGS to seve factors by analysing the outputs of generalized linear models relating the RGDI to seven key factors. Table 2 presents the correlation coefficient results i.e. the mean coefficient values of all statistically significant (z < 0.05) correlated models (denoted as "slope") for four different periods. In whole city scale, GDP shows a significant negative correlation with RGDI, while population shows a significant positive correlation. ISC is negatively correlated with RGDI. Precipitation is shown to have had no statistically significant effect, AMSR, on the other hand, is significantly positively

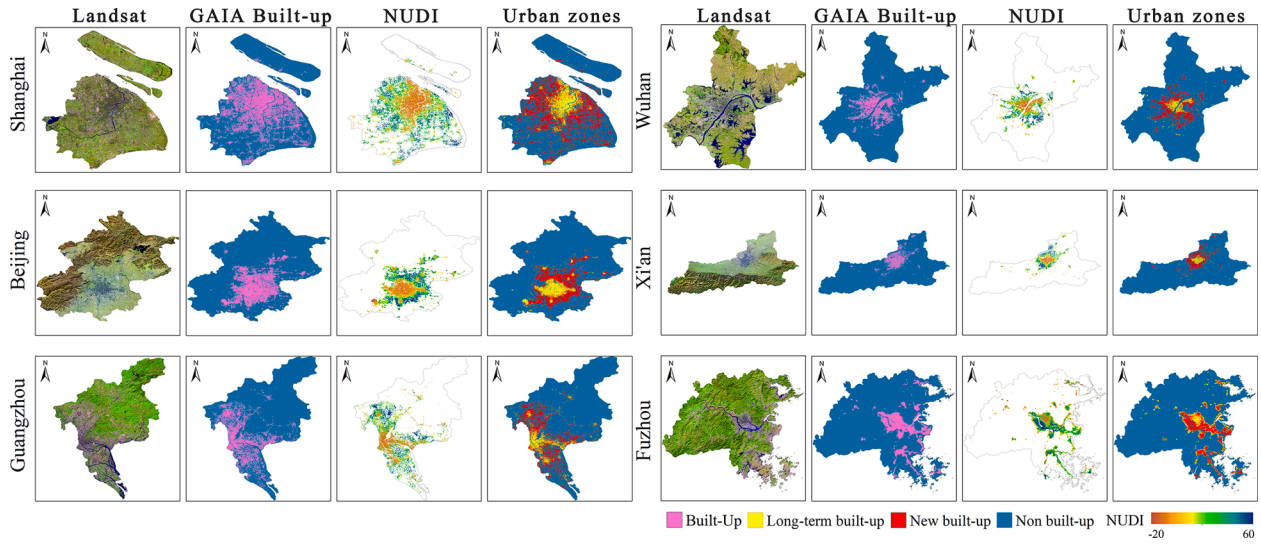

Fig. 3. Spatial distribution of urban development zones based on threshold-based NUDI and GAIA data.

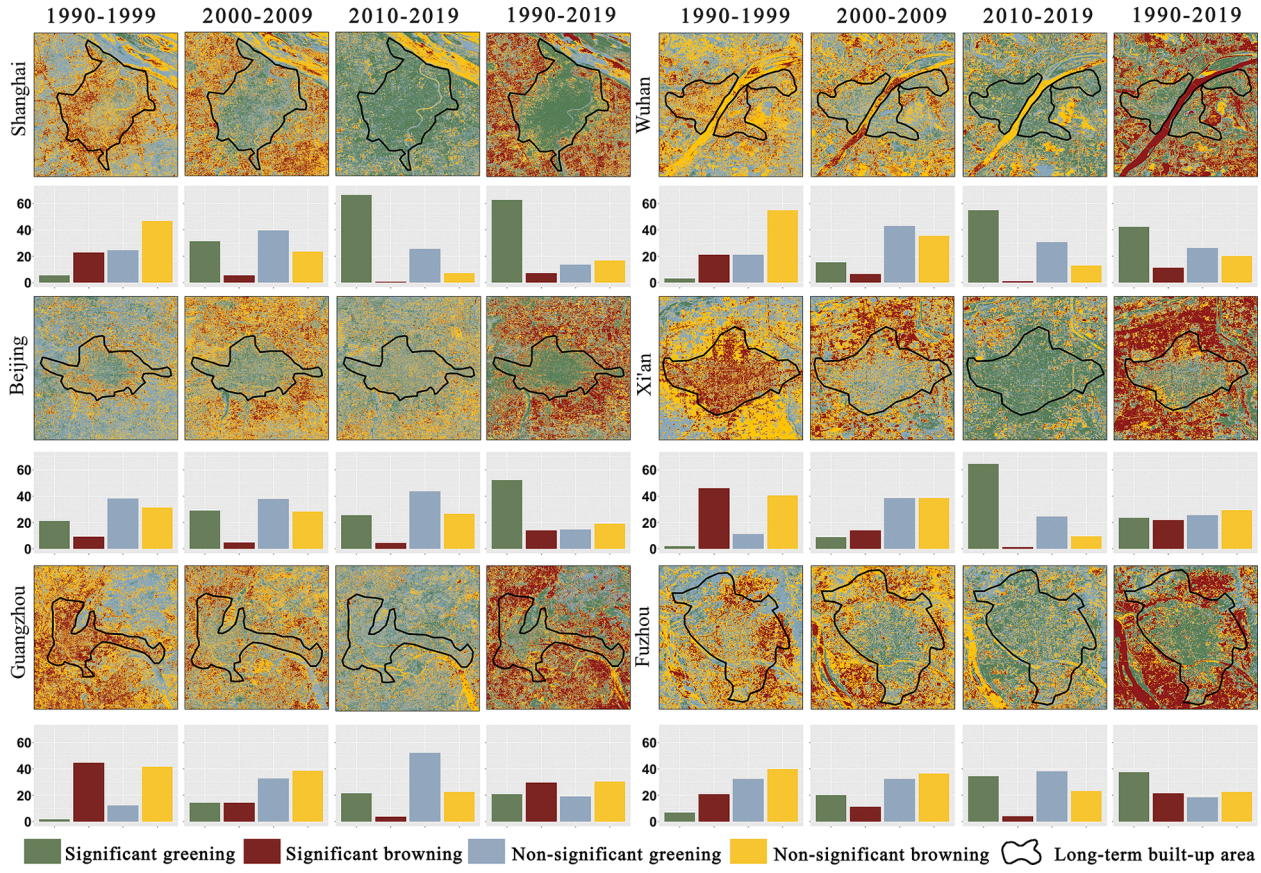

Fig. 4. Dynamics of UGS in long-term built-up for six cities (slope of FVC trend in four temporal periods).

Table 1
Statistics on the sum of SG area and SB area (units are km^2).

Type	LB_SG	LB_SB	NewB_SG	NewB_SB	NB_SG	NB_SB
1990–1999	2,572.97	8,381.66	2,951.68	6,553.18	101,493.07	40,942.84
2000–2009	5,753.32	7,308.54	4,683.38	11,347.28	133,224.62	53,224.76
2010–2019	8,101.80	5,279.45	6,810.22	6,751.67	161,712.93	49,303.65
1990–2019	10,667.52	25,110.43	6,476.69	37,185.50	529,310.47	119,940.32

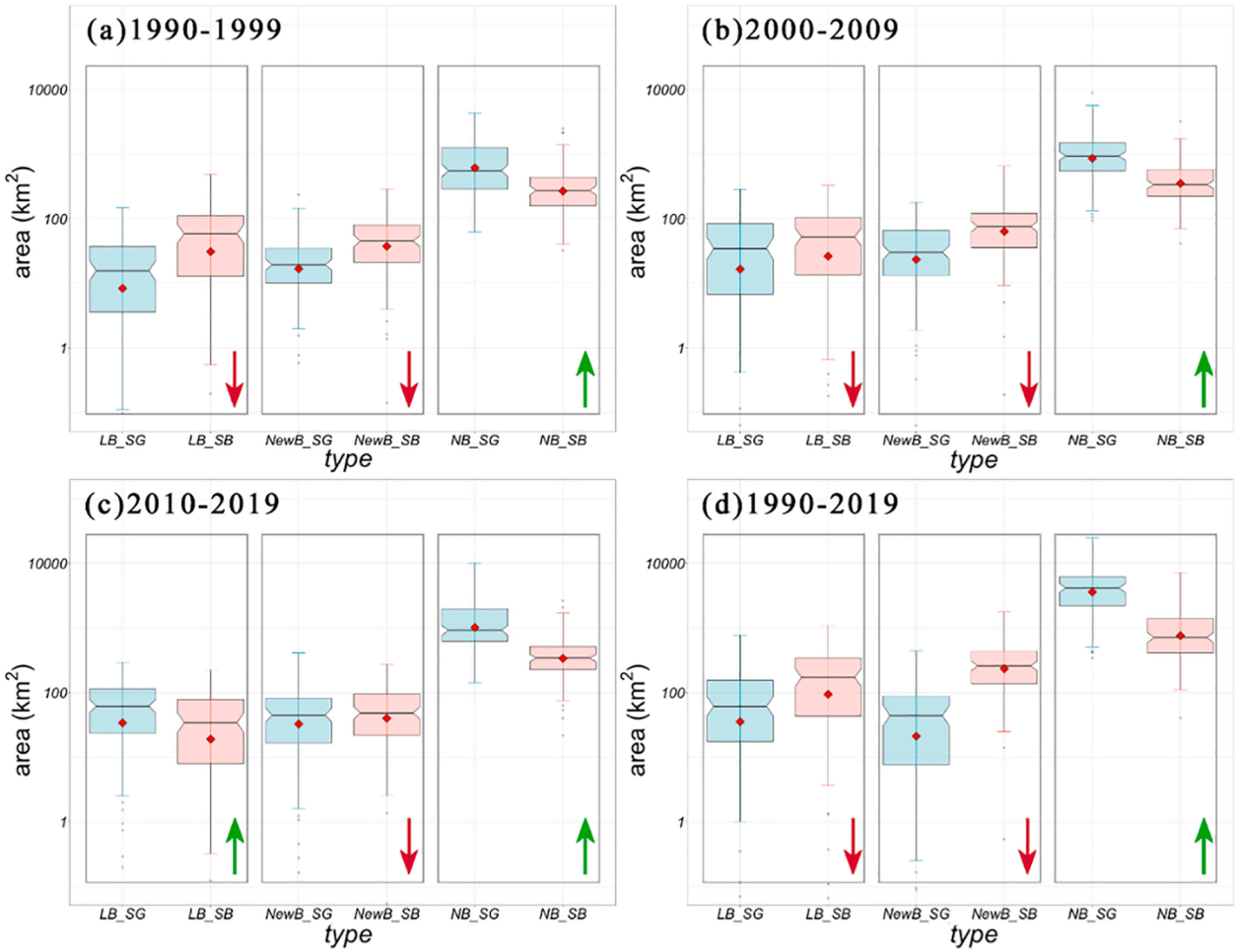

Fig. 5. Statistics for 107 cities with SG and SB areas according to the different zones whereby the position of the red dot indicates the mean area value for all 107 cities, green arrows indicate that the area of significant greening is larger than area of significant browning, and vice-versa for red arrows. Where LB, NewB and NB denote Long-term built-up, New built-up and Non-built-up, respectively. (For interpretation of the references to colour in this figure legend, the reader is referred to the web version of this article.)

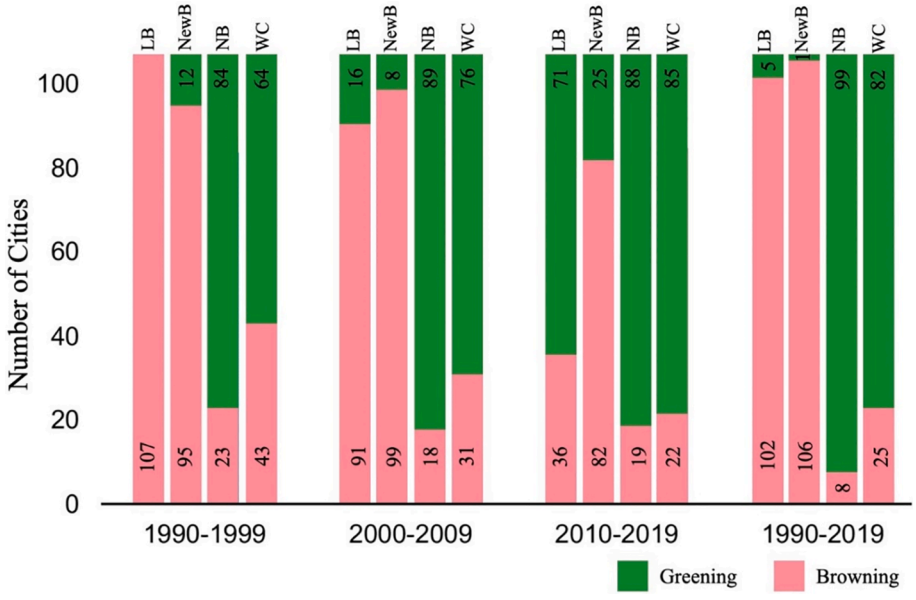

Fig. 6. Statistics on the number of greening and browing cities across time windows for the three different zones, and the city as a whole. Where LB, NewB NB and WC denote Long-term built-up, New built-up and Non-built-up, Whole city, respectively.

Table 2
Regression coefficients between seven variables and RGDI at whole city scale in four different periods.

	GDP	POP	ISC	AMLR	ATP	AMSR	AMT
1990–1999	–	–	−0.25 ***	2.48 ***	–	0.42 **	−2.85 ***
2000–2009	−0.47 ***	0.82 ***	−0.21 *	−0.42 **	0.17	0.29 ***	–
2010–2019	−0.35 *	0.84 ***	−0.37 ***	0.91 *	–	0.26 *	−0.87 .
1990–2019	−0.41 ***	0.64 ***	−0.43 ***	–	–	0.15 *	–

Where "***" represents p-value < 0.001, "**" represents p-value < 0.01, "*" represents p-value < 0.05, and "." represents p-value < 0.1.

correlated and AMT significantly negatively correlated with RGDI.

Results of the BRT analysis show that ISC and POP are the most important factors influencing spatial variation in RGDI in the long-term built-up zone, GDP and ISC are most important in the new built-up zone, while climate change has a much greater impact on RGDI than socio-economic factors in the non-built-up zone. For the city as a whole, ISC and AMSR are important factors influencing the spatial variation of RGDI (Fig. 7).

Correlation analysis of annual regional mean RGDI values and GDP (Fig. 8) indicates that economic growth is associated with significant reductions in UGS between 1990 and 2009. but this relationship then reverses and is significantly positive ($R = 0.62$, $p < 0.01$) between 2010 and 2019. Similarly, economic growth is correlated with reduced greening in the new built-up areas from 1990 to 2010, while also appearing to have promoted greening from 2010 to 2019 ($R = 0.23$, $p < 0.05$). The effects of economic development therefore are shown to vary over time. This is further elucidated in Table 3, which lists the top ten cities, including those most economically highly developed cities in China, with greatest RGDI in the long-term built-up zone over the studied period. Positive growth in both economic development and UGS occurred between 2010 and 2019 and, moreover, the more developed the economy, the greater the degree of greening.

5. Discussion

The spatial analysis of FVC from 1990 to 2019 presented here indicates that the degree of urban browning or greening is related to emerging patterns of urbanization over time. UGS development is markedly uneven, as reflected in the different degrees of urban development within cities and also between cities. Fig. 9 shows the distribution of RGDI in 107 cities in different time periods; the phenomenon of returning to green in the stable built-up areas is obvious during 2010–2019, especially in the Beijing-Tianjin-Hebei city cluster, the Yangtze River Delta city cluster, and the Guangdong-Hong Kong-Macao Greater Bay Area city cluster. For the newly built-up areas, the browning trend is prominent. In contrast, non-built-up areas exhibit a steady greening trend, which is consistent with the findings of previous studies (Chen et al., 2019). While the urban r-greening phenomenon is obvious for the whole city from 1990 to 2019, the Yangtze River Delta urban agglomeration shows a browning trend, which may be due to the replacement of a large amount of urban green space by impervious surfaces as a result of particularly intense urban expansion. Overall, urban expansion and internal densification are associated with browning. However, as witnessed in most Chinese cities after 2009, when urban development matures, the city can begin to recover its UGS. Large-scale urban afforestation projects in China have significantly increased the fraction of vegetation in the established urban areas, improving ecosystem services and enhancing urban sustainability (Yao et al., 2019; Jin et al., 2021; Ding et al., 2021).

Urban green spaces are affected by both climate change as well as socio-economic factors. At the scale of the whole city, precipitation and short-wave radiation are the main climatic factors that promote green space development. Burgeoning urban expansion and urban renewal might be expected to have had a direct and negative impact on UGS. Here we show that the trend of greening in economically developed cities is more significant and that these economically more powerful cities exhibit stronger greening trends than those with lower levels of economic development in long-term built-up area during 2009 to 2019. At the scale of the whole city, economic growth negatively impacts UGS although it is interesting to note that in the older, more established parts of cities, such economic growth seemingly stimulates greening, i.e., the more developed the city economy, the higher the degree of green space optimization in the long-term built-up area. This may be due to the authorities implementation of greening policies, including a range of environmental policies, to promote ecological restoration, including green city construction (Liu et al., 2014; Verdini et al., 2020). Our study also indicates that in built-up areas, the main drivers of green space change are socio-economic factors, while in non-built-up areas, climate-related factors play a dominant role.

The re-greening phenomenon in built-up areas evident over the past decade in this study attests to the initial success of China's urban greening policies and demonstrates that a balance between economic development and ecological civilization is achievable. (Gu et al., 2020).

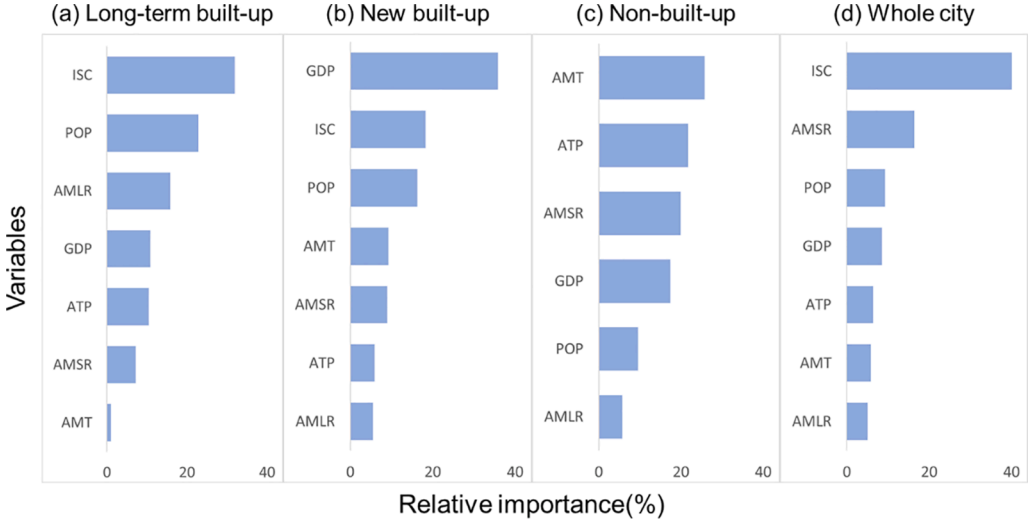

Fig. 7. Ranking of factors affecting RGDI based on BRT analysis.

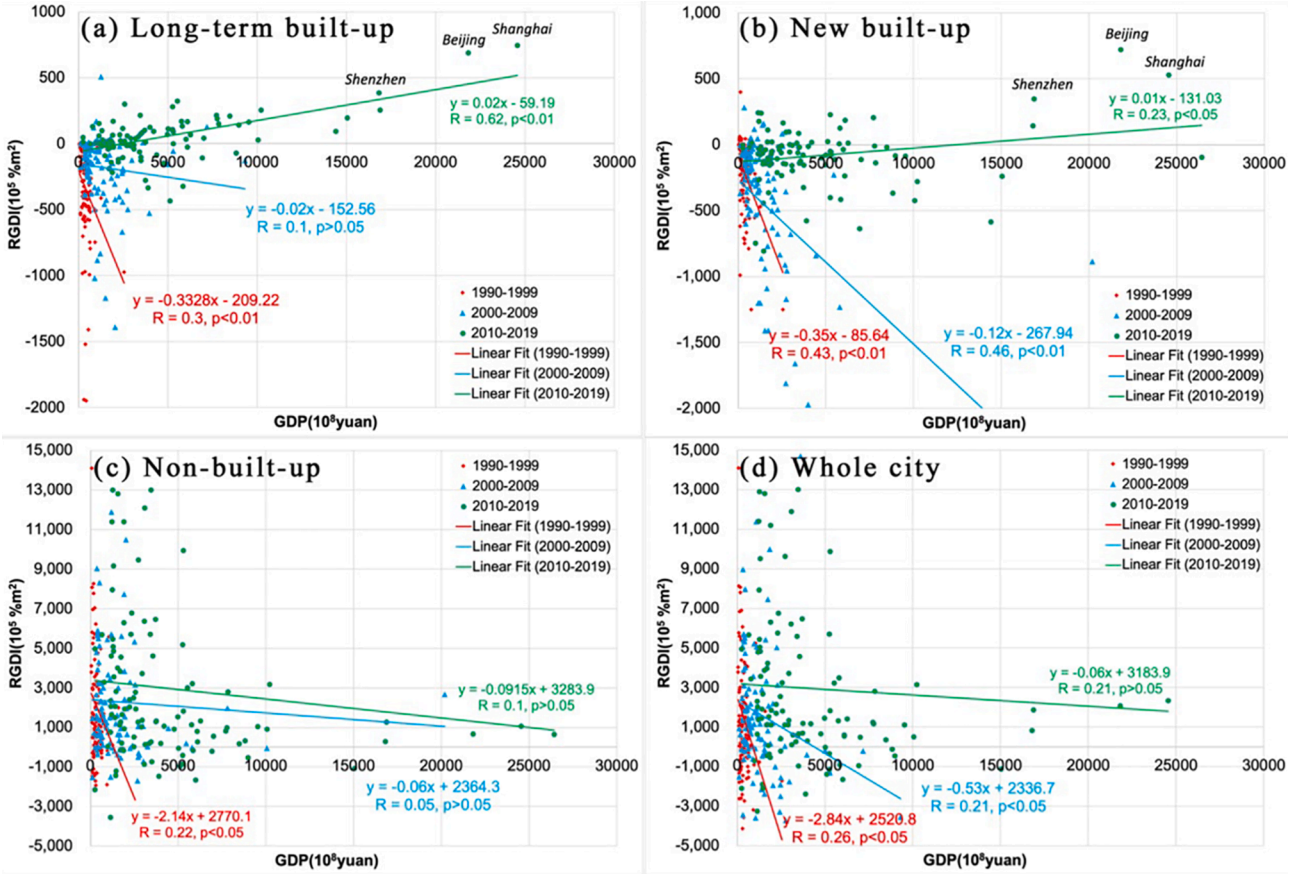

Fig. 8. Relationship between GDP and RGDI in the three zones, and the city as a whole, across four different periods for 107 cities.

Table 3
Ten cities with the highest RGDI in the long-term built-up zone during 2010 to 2019.

City	RGDI (10^7%m^2)	RGDI ranking	GDP (10^8 RMB)	GDP ranking
Shanghai	7.45	1/107	24,558.11	1/107
Beijing	6.89	2/107	21,821.78	2/107
Shenzhen	3.86	3/107	16,812.33	4/107
Xian	3.23	4/107	5,536.78	25/107
Dezhou	3.01	5/107	2,572.00	60/107
Changchun	2.80	6/107	5,261.00	29/107
Guangzhou	2.56	7/107	16,880.33	3/107
Chengdu	2.54	8/107	10,223.33	7/107
Foshan	2.16	9/107	7,725.22	15/107
Jiaxing	2.15	10/107	3,453.56	46/107

More recently, several urban development initiatives at the city and local scale, including “eco-cities”, “national health city”, “low-carbon city and “sponge city” have emerged (Yang et al., 2013; Liu et al., 2009; Li et al., 2017) and have been integrated into ecological spatial planning in the urban context in China. These initiatives all focus on greening in core urban areas and favour further development of gardens and urban parks (The State Council of the People’s Republic of China, 2017). Our findings also provide evidence for the success of policy-driven greening strategies in China’s cities, while providing valuable information for policy makers to assess the historical pattern of urban re-greening. The analysis also highlights that some cities would benefit from a stronger focus on green development policies, such as the national strategy of ecological civilization.

In this study, we applied long time series earth observation remote sensing data to quantify the degree of urban development and define different urban development zones. We demonstrate the application of satellite-derived big data coupled with a comprehensive range of methods to quantify the degree of urban development and urban greening. The methodology enables the reliable assessment of urban development and urban green space dynamics.

6. Conclusions

Using a time-series of remote sensing data it is possible to comprehensively analyse spatio-temporal variations in UGS for across Chinese cities. The data and methods used provide a means to evaluate the dynamics of UGS along a gradient of urban development and to assess possible underlying factors. We undertook spatial analyses for three different zones, including long-term, new, and non-built-up to analyse the development of UGS in 107 major cities in China. NUDI is able more accurately to identify different urban development areas at a higher resolution and therefore provide a more detailed understanding of the effects of different urbanization development stages on UGS. This novel index of urban development offers an efficient means to map the urban-suburban-rural gradient over time and assess the changes in UGS at the regional level. The results of this study highlight several issues that improve existing knowledge of UGS extent and change in revealing spatial differences among different urban development zones. Dynamics of UGS for 107 cities in China across different urban zones are elucidated, along with a consideration of the factors underlying these patterns, i.e. socio-economic conditions, climate, and land use. The analysis reveals signicant differentiation in the effects of these factors over time and in different zones among cities. The methodological toolbox used here is suitable to the evaluation of large data sets with a view to gaining insights to rapid urbanization and its effects on UGS. This study focuses on the quantitative changes in UGS. In order to better explore the dynamics of UGS, future studies should be applied to investigating the

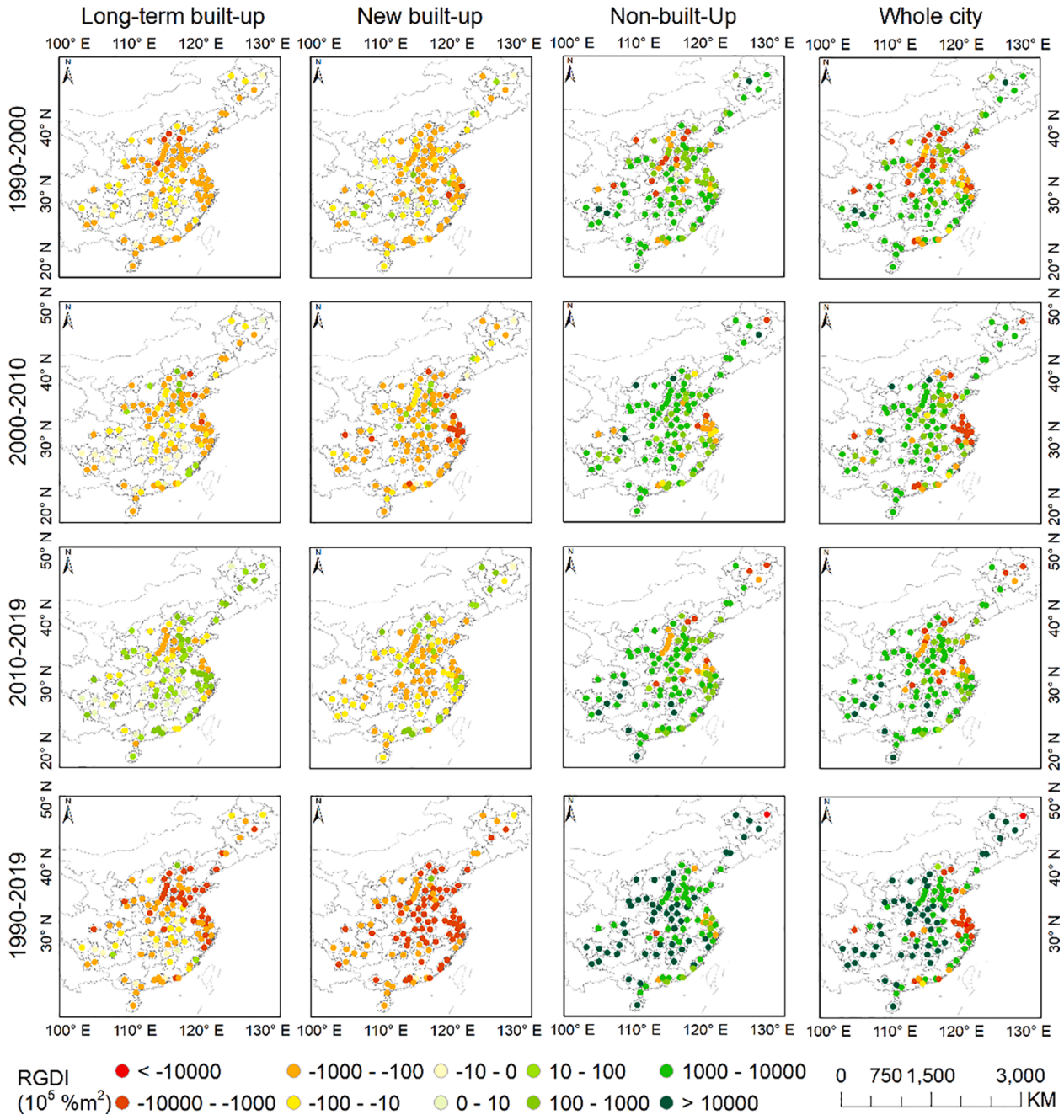

Fig. 9. Spatial and temporal distribution of RGDI for 107 cities in the different zones, and the city as a whole.

effects of urbanization and afforestation projects on attributes such as biodiversity and carbon sequestration capacity of UGS.

Funding

This work is supported by the National Key Research and Development Project of China (grant numbers: 2021YFE0193100, 2018YFD0900806), the Science and Technology Commission of Shanghai, China (grant number: 19DZ1203405), and the European Union's Horizon 2020 research and innovation programme (grant number: 821016).

CRediT authorship contribution statement

Wan-Ben Wu: Conceptualization, Methodology, Writing – original draft. **Jun Ma:** Methodology, Validation. **Michael E. Meadows:** Methodology, Writing – review & editing. **Ellen Banzhaf:** Writing – review & editing, Investigation. **Tian-Yuan Huang:** Software, Validation. **Yi-Fei Liu:** Visualization, Investigation. **Bin Zhao:** Conceptualization, Supervision.

Declaration of Competing Interest

The authors declare that they have no known competing financial interests or personal relationships that could have appeared to influence the work reported in this paper.

References

Bai, T., Mayer, A.L., Shuster, W.D., Tian, G., 2018. The hydrologic role of urban green space in mitigating flooding (Luohe, China). Sustainability 10, 3584.

Barbosa, O., Tratalos, J.A., Armsworth, P.R., Davies, R.G., Fuller, R.A., Johnson, P., Gaston, K.J., 2007. Who benefits from access to green space? A case study from Sheffield, UK. Landscape Urban Plann. 83, 187–195.
Chang, J., Qu, Z., Xu, R., Pan, K., Xu, B., Min, Y., Ren, Y., Yang, G., Ge, Y., 2017. Assessing the ecosystem services provided by urban green spaces along urban center-edge gradients. Sci. Rep. 7, 1–9.
Chen, C., Park, T., Wang, X., Piao, S., Xu, B., Chaturvedi, R.K., Fuchs, R., Brovkin, V., Ciais, P., Fensholt, R., 2019. China and India lead in greening of the world through land-use management. Nat. Sustainability 2, 122–129.
Ding, Z., Zheng, H., Li, H., Yu, P., Man, W., Liu, M., Tang, X., Liu, Y., 2021. Afforestation-driven increases in terrestrial gross primary productivity are partly offset by urban expansion in Southwest China. Ecol. Ind. 127, 107641.
Du, H., Cai, W., Xu, Y., Wang, Z., Wang, Y., Cai, Y., 2017. Quantifying the cool island effects of urban green spaces using remote sensing Data. Urban For. Urban Greening 27, 24–31.
Elvidge, C.D., Tuttle, B.T., Sutton, P.C., Baugh, K.E., Howard, A.T., Milesi, C., Bhaduri, B., Nemani, R., 2007. Global distribution and density of constructed impervious surfaces. Sensors 7, 1962–1979.
Gong, P., Li, X., Wang, J., Bai, Y., Chen, B., Hu, T., Liu, X., Xu, B., Yang, J., Zhang, W., 2020. Annual maps of global artificial impervious area (GAIA) between 1985 and 2018. Remote Sens. Environ. 236, 111510.
Goward, S.N., Markham, B., Dye, D.G., Dulaney, W., Yang, J., 1991. Normalized difference vegetation index measurements from the Advanced Very High Resolution Radiometer. Remote Sens. Environ. 35, 257–277.
Gu, Y., Wu, Y., Liu, J., Xu, M., Zuo, T., 2020. Ecological civilization and government administrative system reform in China. Resour. Conserv. Recycl. 155, 104654.
Gutman, G., Ignatov, A., 1998. The derivation of the green vegetation fraction from NOAA/AVHRR data for use in numerical weather prediction models. Int. J. Remote Sens. 19, 1533–1543.
He, J., Yang, K., Tang, W., Lu, H., Qin, J., Chen, Y., Li, X., 2020. The first high-resolution meteorological forcing dataset for land process studies over China. Sci. Data 7, 1–11.
Hedblom, M., Gunnarsson, B., Iravani, B., Knez, I., Schaefer, M., Thorsson, P., Lundström, J.N., 2019. Reduction of physiological stress by urban green space in a multisensory virtual experiment. Sci. Rep. 9, 1–11.
Jeanjean, A.P., Monks, P.S., Leigh, R.J., 2016. Modelling the effectiveness of urban trees and grass on PM2. 5 reduction via dispersion and deposition at a city scale. Atmos. Environ. 147, 1–10.
Jin, J., Sheppard, S.R., Jia, B., Wang, C., 2021. Planning to Practice: Impacts of Large-Scale and Rapid Urban Afforestation on Greenspace Patterns in the Beijing Plain Area. Forests 12, 316.
Kabisch, N., Strohbach, M., Haase, D., Kronenberg, J., 2016. Urban green space availability in European cities. Ecol. Ind. 70, 586–596.
Kalnay, E., Cai, M., 2003. Impact of urbanization and land-use change on climate. Nature 423, 528–531.
Li, H., Ding, L., Ren, M., Li, C., Wang, H., 2017. Sponge city construction in China: A survey of the challenges and opportunities. Water 9, 594.
Li, X., Gong, P., Zhou, Y., Wang, J., Bai, Y., Chen, B., Hu, T., Xiao, Y., Xu, B., Yang, J., 2020. Mapping global urban boundaries from the global artificial impervious area (GAIA) data. Environ. Res. Lett. 15, 094044.
Liu, H., Zhou, G., Wennersten, R., Frostell, B., 2014. Analysis of sustainable urban development approaches in China. Habitat international 41, 24–32.
Liu, L., Leung, Y., 2015. A study of urban expansion of prefectural-level cities in South China using night-time light images. Int. J. Remote Sens. 36, 5557–5575.
Liu, Z., Dai, Y., Dong, C., Qi, Y., 2009. Low-carbon city: Concepts, international practice and implications for China. Urban Studies 16, 1–7.
McPhearson, T., Maddox, D., Gunther, B., Bragdon, D., 2013. Local assessment of New York City: Biodiversity, green space, and ecosystem services. Urbanization, biodiversity and ecosystem services: Challenges and opportunities. Springer, Dordrecht, pp. 355–383.
Myneni, R.B., Keeling, C., Tucker, C.J., Asrar, G., Nemani, R.R., 1997. Increased plant growth in the northern high latitudes from 1981 to 1991. Nature 386, 698–702.
Otsu, N., 1979. A threshold selection method from gray-level histograms. IEEE transactions on systems, man, and cybernetics 9, 62–66.
Piao, S., Wang, X., Park, T., Chen, C., Lian, X., He, Y., Bjerke, J.W., Chen, A., Ciais, P., Tømmervik, H., 2020. Characteristics, drivers and feedbacks of global greening. Nature Reviews Earth & Environment 1, 14–27.
Richards, D.R., Passy, P., Oh, R.R., 2017. Impacts of population density and wealth on the quantity and structure of urban green space in tropical Southeast Asia. Landscape Urban Plann. 157, 553–560.
Rupprecht, C.D., Byrne, J.A., Ueda, H., Lo, A.Y., 2015. 'It's real, not fake like a park': Residents' perception and use of informal urban green-space in Brisbane, Australia and Sapporo, Japan. Landscape Urban Plann. 143, 205–218.
Silvennoinen, S., Taka, M., Yli-Pelkonen, V., Koivusalo, H., Ollikainen, M., Setälä, H., 2017. Monetary value of urban green space as an ecosystem service provider: A case study of urban runoff management in Finland. Ecosyst. Serv. 28, 17–27.
Verdini, G., Zhang, L., 2020. Urban China: The Tortuous Path Towards Sustainability. Planning Theory & Practice 21, 330–336.
Weng, H., Gao, Y., Su, X., Yang, X., Cheng, F., Ma, R., Liu, Y., Zhang, W., Zheng, L., 2021. Spatial-Temporal Changes and Driving Force Analysis of Green Space in Coastal Cities of Southeast China over the Past 20 Years. Land 10, 537.
Xu, Z., Zhang, Z., Li, C., 2019. Exploring urban green spaces in China: Spatial patterns, driving factors and policy implications. Land Use Policy 89, 104249.
Yang, J., Sun, J., Ge, Q., Li, X., 2017. Assessing the impacts of urbanization-associated green space on urban land surface temperature: A case study of Dalian, China. Urban For. Urban Greening 22, 1–10.
Yang, L., Li, Y., 2013. Low-carbon city in China. Sustainable Cities and Society 9, 62–66.
Yao, N., van den Bosch, C.C.K., Yang, J., Devisscher, T., Wirtz, Z., Jia, L., Duan, J., Ma, L., 2019. Beijing's 50 million new urban trees: Strategic governance for large-scale urban afforestation. Urban For. Urban Greening 44, 126392.
Zhang, Q., Schaaf, C., Seto, K.C., 2013. The vegetation adjusted NTL urban index: A new approach to reduce saturation and increase variation in nighttime luminosity. Remote Sens. Environ. 129, 32–41.
Zhong, Q., Ma, J., Zhao, B., Wang, X., Zong, J., Xiao, X., 2019. Assessing spatial-temporal dynamics of urban expansion, vegetation greenness and photosynthesis in megacity Shanghai, China during 2000–2016. Remote Sens. Environ. 233, 111374.
Zhou, D., Zhao, S., Zhang, L., Liu, S., 2016. Remotely sensed assessment of urbanization effects on vegetation phenology in China's 32 major cities. Remote Sens. Environ. 176, 272–281.
Zhou, X., Wang, Y.-C., 2011. Spatial–temporal dynamics of urban green space in response to rapid urbanization and greening policies. Landscape Urban Plann. 100, 268–277.
Zhou, Y., Wang, Y., 2008. Extraction of impervious surface areas from high spatial resolution imagery by multiple agent segmentation and classification. Photogramm. Eng. Remote Sens. 74, 857–868.